Journal of Applied Polymer Science

Investigations of the Electrical Conduction Mechanisms of Polyaniline-DBSA/Poly(acrylonitrile-butadiene styrene) Blends

Milton Campos,[1] Thiago A. S. Miziara,[1] Fernando H. Cristovan,[2] Ernesto C. Pereira[3]

[1]UNIP—Universidade Paulista, Grupo de Pesquisa "Ciência dos Materiais," Av. Carlos Consoni, 10 CEP 14025-270 Ribeirão Preto, SP, Brazil

[2]UNIFESP—Universidade Federal de São Paulo, Instituto de Ciência e Tecnologia, R. Talin, 330 CEP 12231-280 São José dos Campos, SP, Brazil

[3]Laboratório Interdisciplinar de Eletroquímica e Cerâmica, Departamento de Química, Universidade Federal de São Carlos, CP 676, 13560-970 São Carlos SP, Brazil

Correspondence to: M. Campos (E-mail: campos@unip.br)

ABSTRACT: The electrical properties of Al/PANI-DBSA/ABS/Au blend with PANI (5%) w/w have been investigated by using of current-voltage (I-V) measurements, in a temperature range of 100–313 K. The analysis of I-V characteristics in the forward direction was based on thermionic emission mechanism for applied electrical field till $\sim 3 \times 10^2$ V/cm. The thickness dependence of the current-voltage relationship, clearly demonstrates that the electrical current for larger fields is space charge limited current (SCLC). Temperature dependences of the ideality factor, barrier height, and series resistance have been calculated. The mobility of carriers which is temperature dependent was calculated using the trap free SCLC as 1.53×10^{-4} cm^2 V^{-1} s^{-1} at room temperature. © 2014 Wiley Periodicals, Inc. J. Appl. Polym. Sci. **2014**, *131*, 40688.

KEYWORDS: blends; conducting polymers; kinetics; properties and characterization; thermal properties

Received 15 August 2013; accepted 1 March 2014

DOI: 10.1002/app.40688

INTRODUCTION

Electrically conductive polymeric materials have shown promising commercial viability in technological applications such as electromagnetic shielding (EMI), gas separation membranes, and rechargeable batteries.[1] Therefore, the successful application of these materials to build such devices requires the understanding of charge transport in their bulk as well the charge injection in the interfaces. At present polyaniline (PANI) doped with various protonic acids are one of the most promising materials, because their wide spread applications and high environmental and thermal stability.[2] Several methods of preparation of PANI film such as spin coating, drop coating, electrochemical deposition, thermal evaporation, emulsion polymerization, and Langmuir-Blodgett (L-B) technique[3–5] have been reported. PANI is an important candidate for device application in biosensor and optoelectronics.[6,7] However, PANI has two important limitations, which are low processability and poor mechanical properties. In general, a conducting polymer is not dissolved by common organic solvents due to its large intermolecular interfacial tension. It was reported[8,9] that the use of functionalized protonic acids could dope PANI and enhance its solubility in organic solvents due to the fact that, the molecular interfacial interaction is decreased.[10] An example of such a functionalized acid is camphor sulfonic acid or dodecylbenzene sulfonic acid (DBSA), which has long alkyl chains that increase the solubility of PANI-DBSA in toluene, xylene, *m*-cresol, and chloroform. Also, it acts as a surfactant, inducing compatibility with other polymer matrices with a similar structure. The surfactants are able to cause a drastic conformational change of the random coil polymer. DBSA is anionic surfactant with molecules characterized by a hydrophobic and a hydrophilic group. These blends are normally obtained by mixing soluble or fusible PANI, with other polymers in solutions.[11] In the case of conducting polymers, the generated carriers during the doping process are known to be self trapped by the contacts of the conjugated polymeric chains in the form of polarons or bipolarons.[12] Hence, the electrical conduction mechanism is a complex one and has been explained using different mechanisms propositions such as Mott's variable range hopping, Schottky, Poole-Frenkel, Fowler-Nordheim, space charge limited current (SCLC), and tunneling conduction.[13,14] Usually, one of them may dominate over the others at certain temperature and voltage ranges. However, simultaneous contribution from two or more of them could also be possible, as we are going to show in the present communication.

Considering the exposed above the purpose of this work is to explain the behavior of the experimental forward I-V-T

characteristics of the blend PANI-DBSA/poly(acrylonitrile-butadiene-styrene) (ABS), using the existing electrical conduction models to determine the predominant charge transport mechanism. For that, the junction was prepared by evaporating gold circular electrode on one surface of the blend PANI-DBSA/ABS, whereas aluminum circular electrode of the same area is evaporated on the other surface. Therefore, we have in one side of the sample a rectifying contact (Al) and an ohmic contact in the other side (Au), similar to conventional inorganic semiconductor Schottky barrier diodes, because PANI it is a p-type conducting polymer. These structure is very important because is possible to have, a behavior of thermionic emission theory.

EXPERIMENTAL

Polyaniline in the emeraldine base state (PANI-EB), was chemically synthesized using the polymerization procedure described before.[15] PANI-EB and ABS (GE) (12.5% of acrylonitrile) were dissolved separately with different ratios in a 1 : 4 (v/v) *m*-cresol : chloroform (Aldrich) mixture and stirred for 4 h. Following this, DBSA (Aldrich) (200 μL) was added to the PANI solution and stirred for 2 h. A color change was observed, from blue to green, indicating that PANI was doped by DBSA. The PANI-DBSA solution and the ABS solution were then stirred together for 5 h to obtain the blend. The films were prepared by casting these blend solutions on glass plates. Solvent evaporation was performed at 313 K for 24 h after what the film was easily detached. A PANI-DBSA/ABS composition of 5 wt % PANI were used in all the measurements. It was found experimentally that the percolation threshold for the blend was observed for compositions of 3 wt % PANI.[16] The thicknesses of the prepared blends were typically 10–35 μm, with total active area of about 0.97 cm^2. Gold (5.1 eV) circular electrode of about 0.38 cm^2 was evaporated through a shadow mask on one of the blend surfaces, with vacuum of 10^{-5} Torr, whereas Al (4.28 eV) circular electrode of the same area was vacuum evaporated on the other surface also through a shadow mask.

The Fourier Transform Infrared spectra (FTIR) were recorded from a KBr sample pellet using a Bruker spectrometer, EQUINOX 55 model. The UV–Vis absorption spectra were measured for pure PANI/ABS blend and pure ABS films. These data were recorded using a VARIAN spectrophotometer, CARY model 500. The PANI/ABS blends were also characterized using SEM micrographs with a Zeiss Supra 35VP microscope.

The samples were put in a homemade cell for studying their electrical characteristics. Current-voltage (I-V) measurements were made with the use of a Keithley 6517 electrometer, a Keithley 230 programmable voltage source with the usual two-probe method at temperature range 100–313 K by Lake Shore DRC-93CA temperature controller and computer controlled system trough an IEEE-488 ac/dc card in dark. The sample temperature was always monitored by a copper-constantan thermocouple.

RESULTS AND DISCUSSIONS

The ABS is an insulator polymer, its conductivity[17] is of the order 10^{-9} Scm^{-1}. PANI conductivity can change according to the type of the dopants used or even synthesis procedure. Generally, PANI conductivity[18] can vary from 10^{-4} to 10^{2} Scm^{-1}. Synergism of these two polymers creates a new conductive material with mechanical properties useful in technological application. In a previous work using PANI/ABS blends, it was observed a percolation threshold around 3% (w/w) of PANI.[17] The possibility to prepare devices of the PANI blends, with low PANI amount, of near percolation threshold have provide additional stimulus to carefully study the transport properties of PANI-DBSA network, especially at low volume fractions.

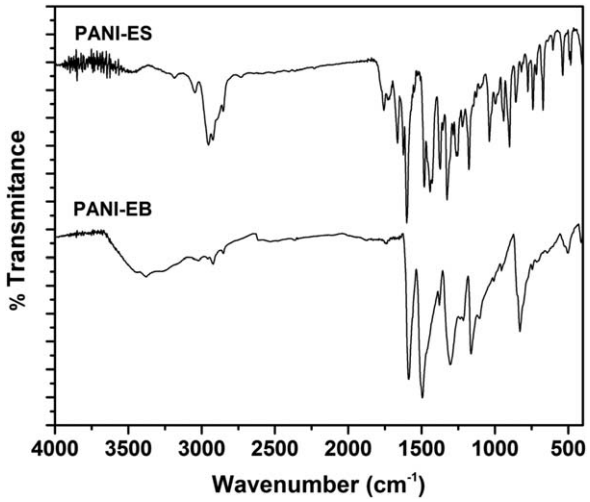

Figure 1. FTIR transmittance spectra of emeraldine salt (PANI-ES) and emeraldine base (PANI-EB). FTIR spectra was recorded using KBr.

FTIR spectroscopy provided valuable information about the polymerization and oxidation state of PANI. Figure 1 presents FTIR spectra of PANI, Emeraldine Salt (ES), and Emeraldine Base (EB). The absorption bands observed for PANI-ES sample are in agreement with the values reported in the literature.[19] The absorption bands between 3450 and 2950 cm^{-1} are attributed to the symmetric deformation of hydrogen in —NH and —CH groups. Generally, the peak at 1600 cm^{-1} was assigned to stretching vibrations of C═C of aromatic ring (benzenoid form). PANI-EB spectrum is also in agreement with the literature.[20,21] In the region between 1105 and 1010 cm^{-1}, as well as between 1500 and 1400 cm^{-1}, the polymer presents strong peaks associated with aromatic ring stretching. Both polymers EB and ES showed two or three broad bands at 3400–3200 and 3150–3100 cm^{-1} due to N—H stretching vibrations of —NH, respectively. Then, it is possible to conclude that the polymerization and the conversion of PANI-ES in PANI-EB was successfully succeeded.

Figure 2(a) shows the UV–Vis absorption spectra of ABS and PANI/ABS blend. ABS practically has no absorption in the 400–2500 nm range. In the 300–400 nm range, there is an increase in the absorption from the aromatic rings of styrene. For PANI/ABS sample, an absorption at 400–440 nm and above 750 nm ranges correspond to polaron-$\pi^{\star}$ and to a $\pi-$polaron band transitions.[22] This indicates that the PANI in blend was in the doped state. Besides, it is important to guarantee that the distribution of PANI in the ABS matrix is homogeneous, once such

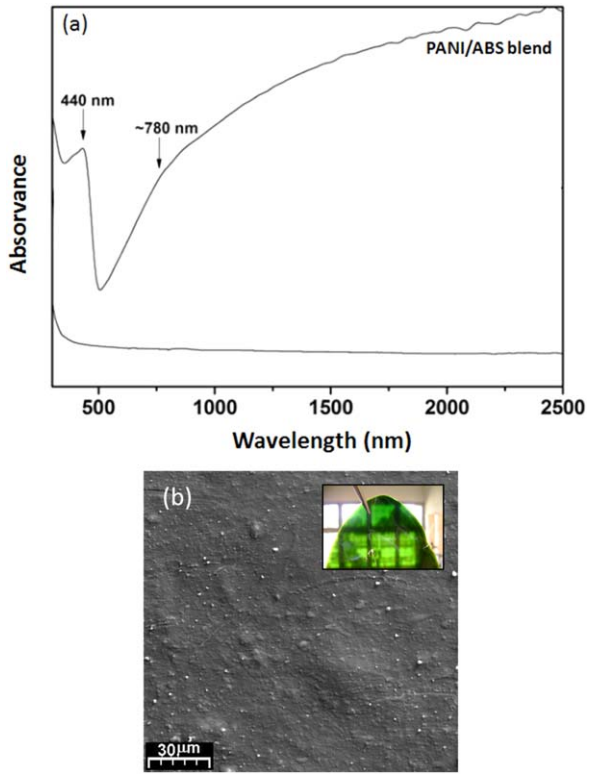

Figure 2. (a) UV-Vis spectra of ABS polymer and PANI/ABS blend. (b) SEM micrographs of PANI/ABS blend. [Color figure can be viewed in the online issue, which is available at wileyonlinelibrary.com.]

parameter can influence the electrical properties of the blends. In Figure 2(b), SEM micrographs of a PANI/ABS blend shows a clearly homogeneous phase.

As it is well established in the literature, the electronic conduction in blends can take place by five different mechanisms. The tunneling one is temperature-independent but depends on the applied voltage. On the other hand, thermionic emission, Poole-Frenkel emission, SCLC, and hopping conduction mechanism depend on temperature. Thus to identify exact conduction mechanism, it is essential that I-V data should be taken over a large voltage range as well as at different temperatures. With this in mind, in the following paragraphs we discuss the obtained results in the light of the possible mechanism of conduction.[23]

The (I-V) characteristic of the Al/PANI-DBSA/ABS/Au structure is shown in Figure 3, for temperature of 300 K. An asymmetric and nonlinear I-V curve shows that the blend exhibits rectification behavior which confirms that the junction between the blend and Al forms a Schottky barrier, but saturation has not been observed in reverse current. At room temperature (300 K), rectification ratio, i.e., ratio of electrical current in forward bias to the electrical current in reverse bias, at ± 1 V was determined to be 10^2. The Schottky barrier was formed at the junction between aluminum and the sample due to the mismatch between the work function of the metal and the highest occupied molecular orbital level of the blend. As we can see from Figure 3, the forward and reverse I-V characteristics are dissimilar. The reverse current values are much lower than the forward current values at the same ambient temperature.

First, we present evidences about those mechanism which can be discarded to explain the results here presented.

Tunneling is a quantum mechanical phenomenon in which an electron passes through a potential barrier without acquiring enough energy to overcome the top of the barrier. It is assumed that the Fermi level in the blend lies above the bottom of the conduction band.

Simmons[24] has shown that the theoretical relationship between tunneling current density and applied voltage is given by

$$J=\left(A/d^2\right)\{[\Phi\ \exp\left(-Bd(\Phi)^{1/2}\right]-(\Phi\ +qV)\ \exp\left[-Bd(\Phi\ +qV)\right]\} \quad (1)$$

where

$$A=q/\left(4\pi^2\xi\hbar\right) \qquad B\ =2\xi\ \left(2m*/\hbar^2\right)^{1/2} \quad (2)$$

q is the electronic charge, m^* is the effective mass, ξ is a constant, $\hbar$ is the reduced Plank constant, Φ the barrier height, d is the barrier width, and V is the voltage.

In the vicinity of $V=0$, we have for the eq. (1):

$$J=[C(\Phi)^{1/2}/d]\ \exp\ \left[-BVd(\Phi)^{1/2}\right] \quad (3)$$

where

$$C=\left[q(2m^*)^{1/2}\right]/\left(4\xi\pi^2\hbar^2\right) \quad (4)$$

As we can see from eq. (3), ln (J) is proportional to the voltage V. If $V>\Phi/q$, eq. (1) reduces to Fowler-Nordheim form[25]

$$J=DE^2\exp\left[-(F/E)\right] \quad (5)$$

where $E=(V/d)$ is the electrical field, $D=(q^3)/(16\pi^3\hbar m^*\Phi)$ and the constant

$$F=\ (2m*)^{1/2}/\left[3q\,\hbar(\Phi)^{3/2}\right].$$

If the electrical current transport is dominated by Fowler-Nordheim tunneling then a plot of $\ln(J/E^2)$ versus $(1/E)$ should show linear behavior. What was observed is that the slope of ln

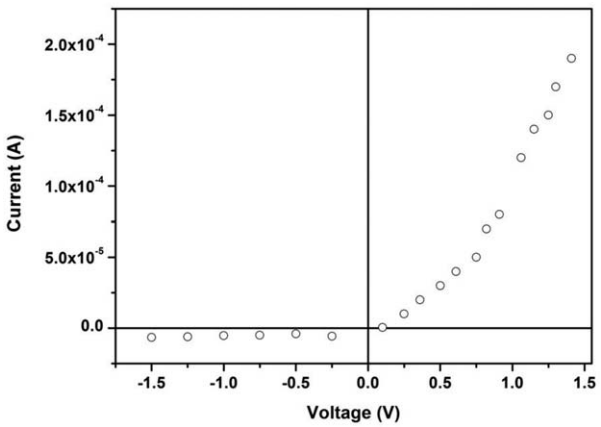

Figure 3. Electrical current as a function of voltage (I-V) at room temperature for a sample of Al/PANI-DBSA/ABS/Au with 5 wt % of PANI, and thickness of 18 μm.

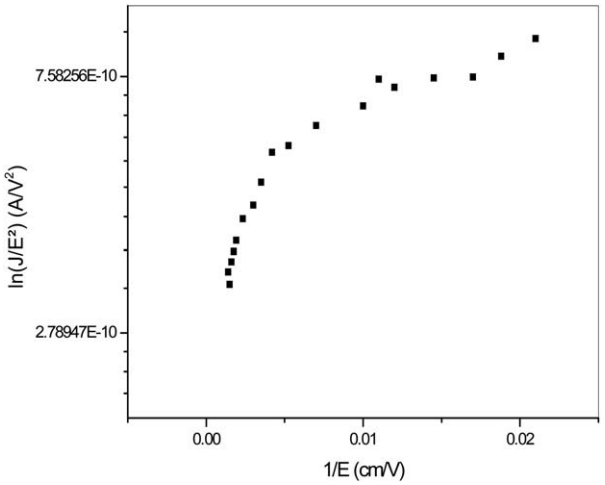

Figure 4. Plot of $\ln(J/E^2)$ versus $(1/E)$ for Al/PANI-DBSA/ABS/Au blend with 5 wt % of PANI, and thickness of 24 μm.

(J) versus V plot for various temperatures was not linear and was not independent of temperature. Also, ln (J/E^2) versus $(1/E)$ was not linear as we can see from Figure 4. Thus, we conclude that it is not possible to explain the experimental results using the current tunneling model.

The Poole-Frenkel effect (bulk limited) is associated with the electric field-enhanced thermal excitation, or detrapping of trapped carriers, which is very similar to the Schottky effect (electrode limited). Both effects are due to the coulombic interaction between the escaping electron and a positive charge. However, they differ in that the positive charge is fixed for the Poole-Frenkel trapping barrier, whereas it is mobile for the Schottky barrier.

The amount of the barrier lowering due to the Poole-Frenkel effect is

$$\Delta E_{\mathrm{PF}} = \left(q^3 E/\pi \in \in_0\right)^{1/2} = \beta_{\mathrm{PF}} E^{(1/2)} \tag{6}$$

where

$$\beta_{\mathrm{PF}} = \left(q^3/\pi \in \in_0\right)^{1/2} \tag{7}$$

The lowering of the potential barrier due to Schottky effect is

$$\Delta E_S = \left(q^3 E/4\pi \in \in_0\right)^{1/2} = \beta_S E^{(1/2)} \tag{8}$$

where

$$\beta_S = \left(q^3/4\pi \in \in_0\right)^{1/2} \tag{9}$$

So comparing eqs. (7) and (9) we have

$$2\beta_S = \beta_{\mathrm{PF}} \tag{10}$$

Using for the dielectric constant[10] a value of 4, we get the calculated values of 6.40×10^{-6} eV $V^{-1/2}$ $m^{1/2}$ for β_S and 3.20×10^{-6} eV $V^{-1/2}$ $m^{1/2}$ for β_{PF}. However, the experimental value of β calculated from the plot of $\ln(I)$ versus $V^{(1/2)}$ was found to be 4.27×10^{-5} eV $V^{-1/2}$ $m^{1/2}$ that is different from the calculated values.

The only comparison between the experimental and theoretical values cannot decide that the dominant conduction mechanism is Poole-Frenkel type. In general, the experimental calculated values of β are larger than the theoretical values. Therefore, the comparison between the theoretical and the experimental values of β does not reveal which mechanism is involved in conduction. To explain the conduction mechanism, it was studied the effect of nature of different electrode material like aluminum, gold and silver. It was observed that the electrical current changed as the contact electrode that was evaporated in both sides of the sample, is different. As the conduction mechanism for Poole-Frenkel type is known to be electrode independent,[26] we can conclude that our results can not be explained by Poole-Frenkel theory.

At this point considering the mechanisms described in the literature, two more possibilities must be investigated: thermionic emission and SCLC. It was observed that the electrical current-voltage (I-V) characteristics are described by different processes, according to the values of the electrical current.

A set of semilogarithmic forward I-V characteristics of the Al/PANI-DBSA/ABS/Au diode measured at different temperatures are shown in Figure 5. This figure shows that the forward diode current is an exponential function of the applied bias in the voltage regime $(0.1 \leq V \leq 0.6$ V), following the thermionic emission mechanism. Starting from this value of bias, the current-voltage characteristics depart from the exponential trend, probably due to the space charge injection from the aluminum contact. Also, it is possible to observe that the ln(I)-V curves are almost parallel which, as consequence, means that the ideality factor is not constant with temperature. It is also observed that the electrical current increased with the increase of temperature for the same applied field.

The forward I-V characteristics of the Schottky diode are generally described by the thermionic emission theory without diffusion and tunneling. The essential assumption of thermionic emission is that an electron from the metal can be injected into the polymer, once it has acquired a thermal energy sufficient to cross the potential maximum that results from the superposition of the external and image charge potential. With application of bias voltages larger than 3 kT/q, the current I,

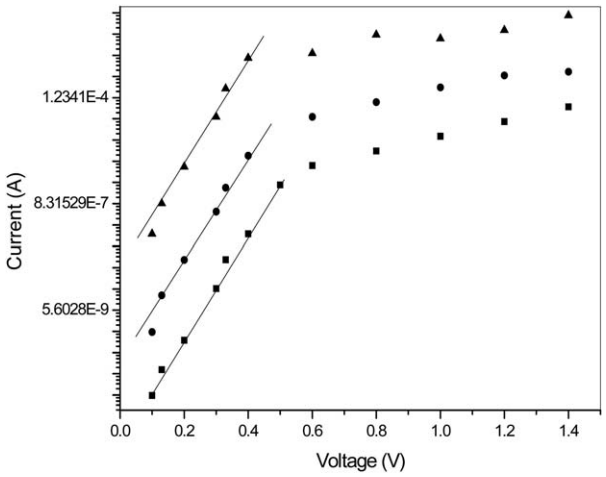

Figure 5. Semilogarithmic forward I-V characteristics of Al/PANI-DBSA/ABS/Au blend with 5 wt % of PANI, and thickness of 13 μm measured at 100 K (■), 180 K (●), and 250 K (▲).

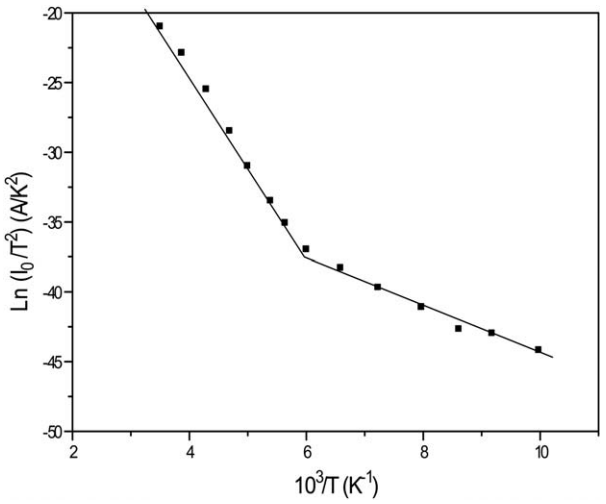

Figure 6. Plot of $\ln(I_0/T^2)$ versus 10^3/T for Al/PANI-DBSA/ABS/Au blend, with 5 wt % of PANI, and thickness of 22 μm.

for an applied voltage V, can be described by the following relation[7]:

$$I = I_0\{\exp\ [q(V - V_S)/nkT] - 1\} \quad (11)$$

where V_S represents the voltage drop across series resistance (R_S) of diode, and n is the ideality factor ($n = 1$ in the ideal case). However, n has usually a value greater than unit. Height values of n can be attributed to the presence of interfacial thin native oxide layer and a wide distribution of barrier height.[27] We attributed the nonideal behavior to effects of bias voltage drop across the interfacial native oxide layer and series resistance. I_0 is the saturation current, which can be expressed as:

$$I_0 = AA * T^2 \exp\ [-q\phi_B/kT] \quad (12)$$

where ϕ_B is the effective barrier height at zero bias, A^* and A are, respectively, the effective Richardson constant and effective diode area. The effective barrier height can be obtained from Richardson plot of the saturation current.

The ideality factor n is determined from the slope of the straight-line region of the semi-log forward bias I-V characteristics through the relation:

$$n = q/kT\mathrm{d}V/\mathrm{d}[\ln(I)] \quad (13)$$

According to eq. (12), if the barrier height ϕ_B is independent of temperature, a linear dependence on the $\ln(I_0/T^2)$ versus T^{-1} curve must be observed. However, for the temperature range 100–313 K the experimental results show two straight lines with different slopes (Figure 6), thus indicating that ϕ_B is temperature dependent, with different behavior for different temperature regions. Besides, the presence of two slopes suggests that two different current transport mechanisms could dominate in these two temperature ranges. Under forward bias and $T < 180$ K, the data for the diode can be fitted with a straight line representing an activation energy of 0.32 eV. Above 180 K, the diode shows a smaller activation energy of 0.11 eV. This result confirms that the predominant current transport is not only the thermionic emission.

Measurements of I-V at different temperatures were made, and the results for n and Φ_B are showed in the Figure 7 and Figure 8, respectively. From these figures, it is noticeable that the barrier height becomes smaller as the ideality factor increases, when the temperature decreases, as was observed before.[8]

The very strong temperature dependence of the ideality factor shows, that the forward bias transport properties are not well modeled only by the thermionic emission even, when it was modified by the incorporation of a series resistance.

Those are the reasons for the increasing of the current density with temperature. Figure 9 shows the experimental series resistance values, as obtained from I-V characteristics as a function of temperature. Using eq. (11) we can see that V_S increases as the temperature increases. It means that the applied V values decrease once they is calculated from the difference

The increase of ideality factor as the temperature decreases is known as T_0 effect.[16] Explanations for that and for variations of the barrier height were proposed, assuming image force[7] and quantum mechanical tunneling.[8] However, if it is due to thermionic-field emission or to the effect of recombination in the depletion region, n will be temperature dependent. The majority of Schottky diodes exhibit n values which depend on temperature. This situation is equivalent to writing $n = 1 + (T_0/T)$ where T_0 is a constant independent of temperature. Therefore, the experimental results imply a sort of temperature dependence of n. The effect is evidently not an intrinsic property of ideal Schottky barriers but an artefact. Various attemps have been made to explain such temperature dependence in termes of particular distribution of interface states[28] and a non-uniformly doped surface layers[29] .The simplest form of barrier lowering is that due to image force. Following the image force model, the variation of barrier height $\Delta\phi_B$ is proportional to the reverse bias $(V_R)^{1/4}$, and consequently a plot of $\ln(I)$ versus $(V_R)^{1/4}$ should give a straight line. However, this behavior was not observed in our measurements, what leads to the conclusion that the variation of barrier height is not due to image force.

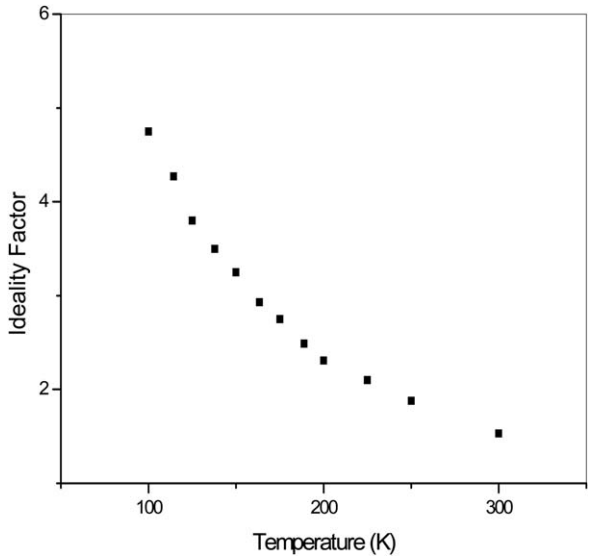

Figure 7. Temperature dependence of ideality factor for Al/PANI-DBSA/ABS/Au blend with 5 wt % of PANI, and thickness of 13 μm.

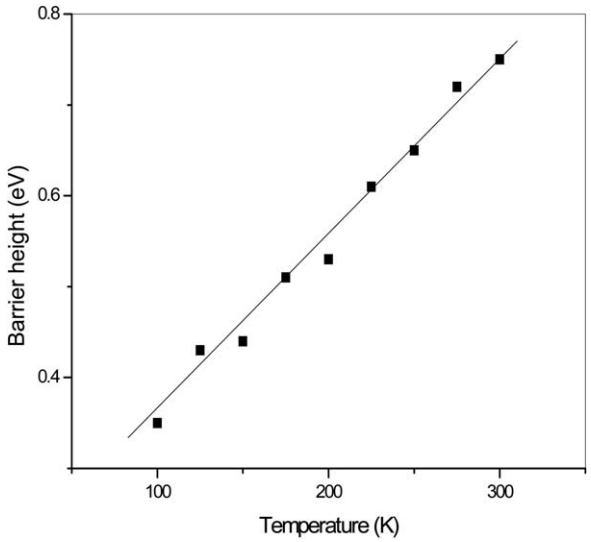

Figure 8. Temperature dependence of barrier height for Al/PANI-DBSA/ABS/Au blend with 5 wt % of PANI, and thickness of 13 μm.

It is very interesting to notice that with the behavior of thermionic emission that was observed in our samples, is possible to obtain electrical currents of mA with small voltages, what is not obtained in others blends. So we can have the possibility of big number of applications, like for example in the area of sensors.[30]

A second possibility to explain the data is the tunneling through the barrier, which is not possible as observed before. Finally, a third proposition could be inhomogenities of the barrier height, interfacial layer at metal-semiconductor interface and/or nonuniformity of the interface charges. Considering the reactivity of Al with the moisture, it is reasonable to assume the formation of a native oxide layer, Al_2O_3 between the blend and aluminum electrode.[9,31]

The SCLC mechanism occurs when an applied voltage originates a non equilibrium density of carriers to be injected in the material. If the voltage is high enough, the trapped carriers contribute to the conduction paths and reliable informations can be deduced from the I-V characteristics. If the amount of injected carriers is larger than the quantity that can be transported across the sample, a space charge will be built at the metal-semiconductor interface. Electrons flowing through the system under an electric field will be impeded and controlled by the space charge collected at the interface what gives rise to SCLC. In this model, the injected current is independent of the mechanism of carrier generation and depends only on the transport interface and trapping of the carriers within the sample. SCLC mechanism can be observed in polymer devices, when one of the device contacts is ohmic.[9] SCLC occurs when the transit time of any excess injected carrier is less than the bulk dielectric relaxation time. Under these circunstances, the trap free SCLC takes the simple form of Child's law, as we can see in the eq. (14). Note that this does not necessarily imply the absence of traps in the material, but rather that they are all filled.

In this case, the equation relating the electrical current to the voltage is

$$I = 9A\epsilon\ \mu_{ef}\ V^2/(8d^3) \tag{14}$$

where A is the effective diode area, ϵ the permittivity of the blend PANI-DBSA/ABS, μ_{ef} the effective mobility of carriers in the blend, and d the blend thickness. To test the validity of the SCLC theory, eq. (14) is written more simply as

$$I = BV^m \tag{15}$$

By comparing eq. (14) with eq. (15), we have

$$B = 9A\epsilon\mu_{ef}/(8d^3) \text{ and } m = 2. \tag{16}$$

In Figure 10, a plot of I against V^2 is reported, showing a linear fitting for three temperatures. Using the value of B obtained from this plot and the value of 4 for the dielectric constant[10] at room temperature, a value of $\mu_{ef} = 1.53 \times 10^{-4}$ cm^2 V^{-1} s^{-1} was calculated. To the best of our knowledge the value for the blend mobility of Al/PANI-DBSA/ABS/Au was not calculated before.

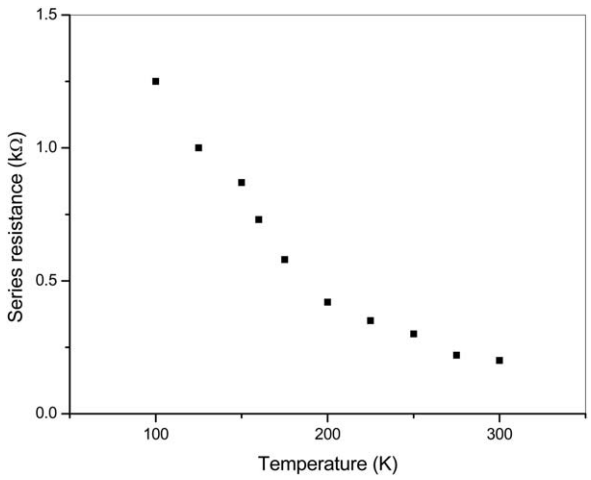

Figure 9. Electrical series resistance obtained from semilogarithmic (I-V) characteristics as a function of temperature for Al/PANI-DBSA/ABS/Au blend with 5 wt % of PANI, and thickness of 17 μm.

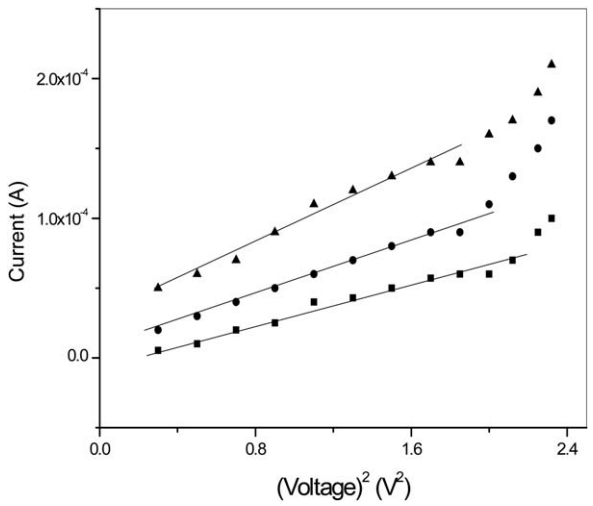

Figure 10. Electrical current as a function of V^2 for Al/PANI-DBSA/ABS/Au blend with 5 wt % of PANI, and thickness of 19 μm for the temperatures of 160 K (■), 200 K (●), 240 K (▲).

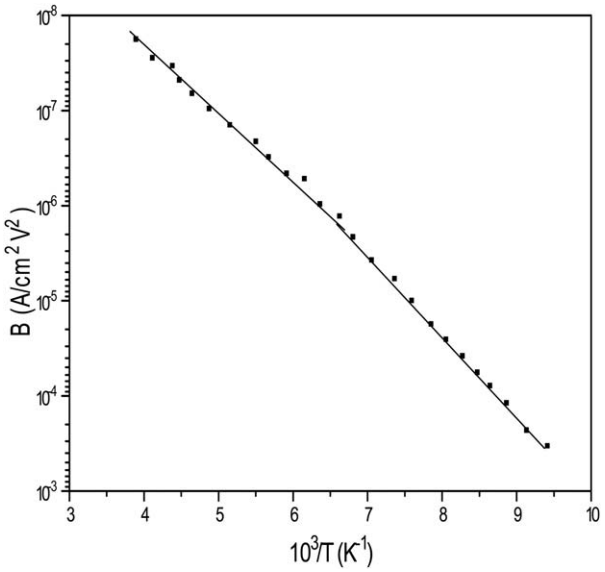

Figure 11. Semilogarithmic plot of B as a function of T^{-1} for Al/PANI-DBSA/ABS/Au blend with 5 wt % de PANI, and thickness of 19 μm.

At high electrical current values, where the current is space charge limited, an increase in forward current with temperature was also observed (Figure 3). From Figure 11 which shows the dependence of log B with $T^{(-1)}$, it can be deduced that B is thermally activated with two different activations energies, 0.52 eV and 0.036 eV. From eqs. (14) and (15), it can be concluded that the mobility is temperature dependent, probably due to the filling of shallow traps. The trap level observed in these experiments may arise from structural imperfections of the blend. As shown in Figure 11, transition between the two activation energies has taken place at ~180 K, probably due to the existence of two different processes of carrier transport in the two different regions as observed before. From space-charge theory, we expect $B \propto d^{(-3)}$ as represented in eq. (16). This was confirmed from the linear dependence in the plot of B vs $d^{(-3)}$ (Figure 12).

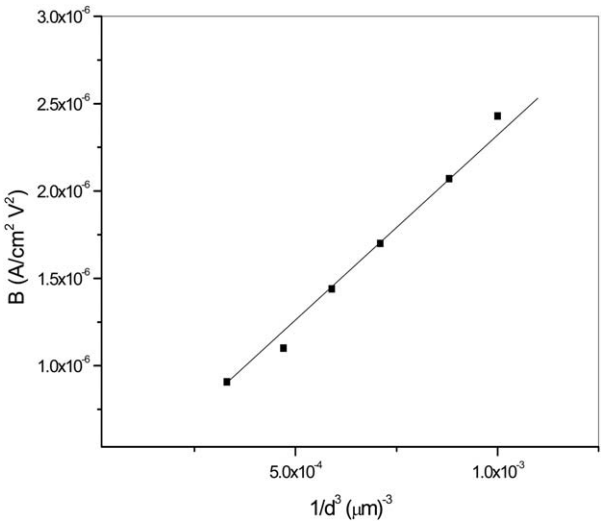

Figure 12. Semilogarithmic plot of B as a function of d^{-3} for Al/PANI-DBSA/ABS/Au blend with 5 wt % of PANI, and thickness of 19 μm.

This indicates that, with high forward currents, carrier transport through the Al/PANI-DBSA/ABS/Au blend is limited by space-charge effects.

CONCLUSIONS

The forward bias I-V characteristics of the Al/PANI-DBSA/ABS/Au blend were measured in the wide temperature range of 100−313 K. The (I-V) curves of the diode exhibit two regions, what can be successfully explained on the basis of the thermionic emission and SCLC mechanism. The temperature dependence of the mobility suggests an activated behavior for charge transport. The value obtained for the mobility at room temperature was 1.53×10^{-4} cm^2 V^{-1} s^{-1}. Experimental results reveal a decrease in barrier height and an increase in the ideality factor n with decreasing temperature, probably due to the drop of applied voltage in interfacial layer.

ACKNOWLEDGMENTS

The authors F. H. C, E. C. P wish to thank the Brazilian research funding institutions CNPq, CAPES, FINEP, and FAPESP. The authors M. C, T. A. S. M acknowledge the support of FAPESP and Vice-Reitoria de Pós-Graduação e Pesquisa da Universidade Paulista (UNIP).

REFERENCES

1. Sivakkumar, S. R.; Kim, D. W. *J. Electrochem. Soc.* **2007**, *154*, A134.
2. Weerakoon, K. A.; Shu, J. H.; Park, M. K.; Chin, B. A. *J. Solid State Sci. Technol.* **2012**, *1*, Q100.
3. Cristovan, F. H.; de Paula, F. R.; Lemos, S.; de Oliveira, A. J. A.; Pereira, E. C. *Synth. Met.* **2009**, *159*, 2188.
4. Chen, X.; Cadmus, C. A.; Wong, K. Y. C.; Ye, H.; Leung, S. Y. Y.; Zhang, G. *Sens. Actuat. B* **2012**, *174*, 210.
5. Mo, Z.; Qiu, W.; Yang, X. C.; Yan, J.; Z. Gu. *J. Polym. Res.* **2009**, *16*, 39.
6. He, X.; Qiu, W. *Chem. Mater.* **2002**, *14*, 2158.
7. Acar, S.; Karadeniz, S.; Tugluoglu, N.; Selçuk, A. B.; Kasap, M. *Appl. Surf. Sci.* **2004**, *233*, 373.
8. Matsuguchi, M.; Io, J.; Sugiyama, G.; Sakai, Y. *Synth. Met.* **2002**, *128*, 15.
9. Campos, M.; Simões, F. R.; Pereira, E. C. *Sens. Actuators B.* **2007**, *125*, 158.
10. Kline, R. J.; Mcgehee, M. D. *J. Macromol. Sci. Polym. Rev.* **2006**, *46*, 27.
11. Abdel-Malik, T. G.; Motaweh, H. A.; Abdel-Hamed, M. O. *J. Photon. Energy* **2011**, *1*, 011116.
12. Lange, U.; Roznyatovskaya, N. V.; Mirsky, V. M. *Anal. Chim. Acta* **2008**, *614*, 1.
13. Robeson, L. M. Polymer Blends: A Comprehensive Review; Hanser Verlag: Munich, Germany, **2007**.
14. Liang, G.; Cui, T.; Varahramyan, K. *Microelectr. Eng.* **2003**, *65*, 279.
15. Özer, M.; Yildiz, D. E.; Altindal, S.; Bülbül, M. M. *Solid-State Electron.* **2007**, *51*, 941.

16. Feng, Y.; Verboncoeur, J. P. *Phys. Plasmas* **2006**, *13*, 073105.
17. Cristovan, F. H.; Lemos, S. G.; Pereira, E. C. *J. Appl. Polym. Sci.* **2010**, *116*, 825.
18. Frommer, J. E.; Chance, R. R. In Encyclopedia of Polymer Science and Engineering; Mark, H. F.; Bikales, N. M.; Overberg, C. G.; Menges, G., Eds.; John Wiley: New York, Vol. *5*, **1986**, p 462.
19. Angelopolus, M.; Dipietro, R.; Zheng, W. G.; MacDiarmid, A. G. *Synth. Met.* **1997**, *84*, 35.
20. Chiang, J. C.; MacDiarmid, A. G. *Synth. Met.***1986**, *13*, 193.
21. Wang, B.; Tang, J.; Wang, F. *Synth. Met.* **1995**, *18*, 323.
22. Stafstrom, S.; Bredas, J. L.; Epstein, A. J.; Woo, H. S.; Tenner, D. B.; Huang, W. S.; MacDiarmid, A. G. *Phys. Rev. Lett.* **1987**, *59*, 1464.
23. Karatas, S.; Altindal, S. *Mater. Sci. Eng. B* **2005**, *122*, 133.
24. Simmons, J. G. *J. Appl. Phys.* **1963**, *34*, 2581.
25. Fowler, R. H.; Nordheim, L. *Proc. R. Soc. A* **1928**, *119*, 173.
26. Ohring, M. The Materials Science of Thin Films, Academic Press: San Diego, **1992**.
27. Olbrich, A.; Vancea, J.; Kreupl, F.; Hoffmann, H. *J. Appl. Phys.* **1998**, *83*, 358.
28. Demirezen, S.; Sönmez, Z.; Aydemir, U.; Altindal, S. *Curr. Appl. Phys.* **2012**, *12*, 266.
29. Roy, S. B.; Daw, A. N. *Solid-State Electron.* **1980**, *23*, 949.
30. Bai, H.; Shi, S. *Sensors* **2007**, *7*, 267.
31. Shakoor, A.; Rizvi, T. Z.; Sulaiman, M.; Nasir, M.; Ishtiag, M. J. *J. Mater. Sci. Mat. Electron.* **2010**, *21*, 603.